SCIENCE CHINA
Information Sciences

• RESEARCH PAPER •

November 2016, Vol. 59 112209:1–112209:14
doi: 10.1007/s11432-015-0153-2

Second-order sliding mode attitude controller design of a small-scale helicopter

Shuai TANG[1*], Li ZHANG[1], Shaoke QIAN[2] & Zhiqiang ZHENG[2]

[1]*Department of Machinery & Electrical Engineering, Logistical Engineering University, Chongqing* 401311*, China;*
[2]*College of Mechatronic Engineering and Automation, National University of Defense Technology, Changsha* 410073*, China*

Received December 7, 2015; accepted January 15, 2016; published online October 14, 2016

Abstract In this paper, the attitude control of a small-scale helicopter is investigated. The main rotor flapping dynamics is explicitly explored to improve the control performance. A two-layer control architecture is adopted: the inner loop controller is designed combining second-order sliding mode control with extended state observer to control the angular rates and yield good robustness properties with respect to model uncertainties; the outer loop controller is used to control the attitude. Experimental results show that the proposed controller yields excellent performance and robustness.

Keywords small-scale helicopter, second-order sliding mode, extended state observer, disturbances, robustness

Citation Tang S, Zhang L, Qian S K, et al. Second-order sliding mode attitude controller design of a small-scale helicopter. Sci China Inf Sci, 2016, 59(11): 112209, doi: 10.1007/s11432-015-0153-2

1 Introduction

Small-scale helicopters can vertically take off and land, hover, turn on the spot, move in various directions, and cruise similar to fixed-wing vehicles. These characteristics have made them indispensable for a variety of applications, such as border patrol, intelligent traffic monitoring, rescue services, 3D mapping, power line inspection, fire front monitoring, and so on [1–5]. However, it is more difficult to control a small-scale helicopter than its full-scale counterpart due to the faster dynamics and higher sensitivity to the control inputs and external disturbances. Although basic autonomous flight has been achieved, the performance is indeed modest in comparison with a skilled pilot and can not satisfy the requirements of some advanced applications. Meanwhile, the robustness of the controllers also needs to be improved. Therefore, designing a robust flight controller which can take full advantage of such vehicle is still an attractive research topic.

Traditional approaches for small-scale helicopters flight control involve linearization at a set of pre-selected equilibrium or trim points within the flight envelop. The final control law is synthesized using gain-scheduling. The major advantage is that minor computations are required and many linear control design techniques are available, such as PID [6,7], LQR [8,9], and H_∞ method [10,11]. However, a linear model is only valid in the neighborhood of the trim point. When the operating point of the helicopter

* Corresponding author (email: tangshuai@nudt.edu.cn)

moves away from the design trim point, performance may be degraded severely and the closed-loop system may be even unstable.

Recently, many researchers have devoted much attention to nonlinear control techniques to overcome the theoretical limitations and drawbacks of linear controllers. Backstepping is a systematic and recursive nonlinear control design technique and has been widely used for small-scale helicopters. In [12] and [13], the authors developed the velocity and position tracking controller, respectively, based on a similar backstepping control of a general rigid body. However, the main rotor flapping dynamics was not considered. Ref. [14] presented an adaptive backstepping controller for hover mode. Although the flapping dynamics and servo dynamics were both considered in the control design, the authors did not provide any observer design for flapping angle estimation, which is important for practical implementation. Based on [15], a backstepping controller was completed using dynamic extension incorporating with recurrent neural network in [16], which treated the thrust of the main rotor and its first derivative as the state variables of the system, and the moment and the second-order derivative of the thrust as system inputs. But neither the flapping dynamics nor main rotor aerodynamics was considered. Sliding mode control is a nonlinear robust control method which employs a control action across a sliding surface to eliminate the effect of uncertainty and has been widely used for nonlinear control system design [17–19]. Ref. [20] proposed a novel nonlinear control approach based on sliding mode control. This approach is applied to a small-scale helicopter to deal with the model uncertainties and external disturbances. The flapping dynamics is explicitly considered, but the immeasurability of the flapping angles are disregarded. Some other methods also have been adopted to design flight controllers, which include neural networks [21], feedback linearization [22], composite nonlinear feedback control [23], and model predictive approach [24, 25], to name a few.

The attitude control problem for a small-scale helicopter is quite challenging. Beside the attitude kinematics and the rotation dynamics, the flapping dynamics corresponding to the tilting motion of the main rotor should also be considered. Flapping dynamics is a unique feature of helicopters which can be expressed by flapping angles. For the control design of small-scale helicopters, flapping dynamics is a specially important factor because the stabilizer bar, equipped to provide lagged rate feedback to facilitate manual operation, substantially renders a lightly damping feature in the rotation dynamics, which decreases the damping ratio and reduces stability [26]. Disregarding flapping dynamics and treating it as a quasi steady state equation is a practical method in the existing literature [16, 24, 27]. Meanwhile, two second-order notch filters are used in the roll and pitch control channels to compensate for the aforementioned lightly damping phenomena. But this method will limit the control performance at higher bandwidths. Adopting flapping angles feedback can change the damping ratio. However, the flapping angles cannot be directly measured. Moreover, it is difficult to design an observer for estimation due to the complexity of the main rotor aerodynamics.

In this work, a novel control method is proposed to improve the robustness, which adopts the second-order sliding mode method [17, 18] incorporating with extended state observer. A two-layer control architecture is adopted. The inner loop controller is designed to control the angular rates and the flapping dynamics is explicitly considered. The outer loop controller is used to control the attitude.

The remainder of the paper is organized as follows. In Section 2, the nonlinear model of the small-scale helicopter used for controller design is presented. The roll and pitch controller design is presented in Section 3. Several flight simulations and experiments are carried out in Section 4 to validate the performance of the proposed controller. At last, some conclusions are drawn in Section 5.

2 Nonlinear model of a small-scale helicopter

This research is bsed on a Raptor 90 RC hobby helicopter platform, which has a 1.605 m span and a 1.410 m length, as shown in Figure 1. It has a two-blade teetering rotor augmented with a Bell-Hiller stabilizing bar. Five digital servo actuators drive the helicopter. The lateral and longitudinal servo motors are used to control roll and pitch motions through swashplate tilting, the collective motor is used

Figure 1 Small-scale helicopter system.

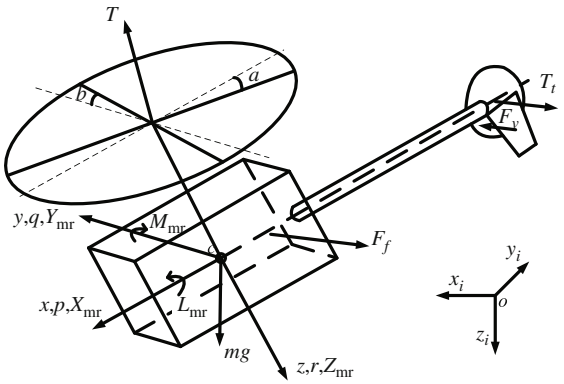

Figure 2 Working principle of a small-scale helicopter.

to control the collective pitch of the main rotor. The onboard avionics includes a sensor packet, flight control board, and wireless communication modem. The sensor packet consists of an AHRS, named MTi, a GPS receiver, and a barometric altimeter. MTi can provide three-axis accelerations, three-axis angular rates and three-axis earth-magnetic field data. Position and velocity can be estimated by fusing data from the GPS receiver and MTi. The flight control board is designed based on a digital signal controller, named TMS320F28335, used to implement the control law and collect all the data to a 4GB SD card. The wireless communication modem is used to monitor the status of the helicopter.

In this work, a hybrid model is used to describe the dynamics of a small-scale helicopter, which includes the nonlinear rigid body dynamics, main rotor dynamics, and simplified yaw dynamics. The model uncertainties and other trivial factors are treated as external disturbances. The position of the gravity center of the helicopter is notated by $P = [x, y, z]^{\mathrm{T}}$ in the inertial frame, where the linear velocity of the gravity center in the inertial frame is given by $v = [v_x, v_y, v_z]^{\mathrm{T}}$ (see Figure 2). Control forces and moments originate mainly from the main and tail rotors, controlled by four inputs: lateral and longitudinal cyclic rotor controls δ_{lat}, δ_{lon}; collective pitch input δ_{col}; and tail rotor collective input δ_{ped}. δ_{lat} and δ_{lon} are used to control roll and pitch motions through swashplate tilting. The rotation speed of the main rotor is controlled by an engine governor and it is not considered. The magnitude of the thrust is controlled by changing the collective pitch angle of the main blades through δ_{col}. δ_{ped} is used to control the yaw angular rate and heading. For the orientation, we take advantage of roll(ϕ), pitch(θ), and yaw(ψ) representation defining $\Theta = [\phi, \theta]^{\mathrm{T}}$ and $\eta = [\phi, \theta, \psi]^{\mathrm{T}}$. The angular velocity of the helicopter represented in the body frame is $\omega = [\omega_1, r]^{\mathrm{T}}$, where $\omega_1 = [p, q]^{\mathrm{T}}$. Actually, using the Euler angles to represent the attitude kinematics, there are singularities when the pitch angle equals to $\pm 90°$. In this paper, it is assumed that ϕ and θ are far away from $\pm 90°$.

The nonlinear rigid body dynamics of the fuselage can be derived by Newton-Euler equation and written as

$$\begin{cases} \dot{P} = v, \\ m\dot{v} = R(\eta)F_b + mge_3, \\ \dot{\eta} = \pi(\Theta)\omega, \\ I\dot{\omega} = -\omega \times I\omega + M_b, \end{cases} \tag{1}$$

where m is the mass of the body, $I = \mathrm{diag}\{I_{xx}, I_{yy}, I_{zz}\}$ is the inertia matrix, g is the gravity acceleration and e_3 is a unit vector along z axis of the inertial frame. F_b and M_b are the control force and moment expressed in the body frame. The rotation matrix from the body frame to the inertial frame $R(\eta)$, and the attitude kinematic matrix $\pi(\Theta)$ are defined, respectively, as

$$R(\eta) = \begin{bmatrix} \mathrm{c}\theta\mathrm{c}\psi & \mathrm{s}\phi\mathrm{s}\theta\mathrm{c}\psi - \mathrm{c}\phi\mathrm{s}\psi & \mathrm{c}\phi\mathrm{s}\theta\mathrm{c}\psi + \mathrm{s}\phi\mathrm{s}\psi \\ \mathrm{c}\theta\mathrm{s}\psi & \mathrm{s}\phi\mathrm{s}\theta\mathrm{s}\psi + \mathrm{c}\phi\mathrm{c}\psi & \mathrm{c}\phi\mathrm{s}\theta\mathrm{s}\psi - \mathrm{s}\phi\mathrm{c}\psi \\ -\mathrm{s}\theta & \mathrm{s}\phi\mathrm{c}\theta & \mathrm{c}\phi\mathrm{c}\theta \end{bmatrix}, \quad \pi(\Theta) = \begin{bmatrix} 1 & \mathrm{s}\phi\mathrm{t}\theta & \mathrm{c}\phi\mathrm{t}\theta \\ 0 & \mathrm{c}\phi & -\mathrm{s}\phi \\ 0 & \mathrm{s}\phi/c\theta & \mathrm{c}\phi/c\theta \end{bmatrix}, \tag{2}$$

where the compact notation c denotes for cos(⋆), s for sin(⋆) and t for tan(⋆).

Flapping dynamics is the main source of the control moment, which is a unique characteristic of helicopters. For a small-scale helicopter, the dynamics of the stabilizer mounted on the main rotor to facilitate manual operation should also be considered. The main rotor flapping dynamics has been modeled in [28] as follows:

$$\begin{aligned}
\begin{bmatrix}\dot{a}\\ \dot{b}\end{bmatrix} &= \frac{\gamma^m\Omega}{(\gamma^m)^2+64}\begin{bmatrix} -\frac{4k_\beta}{I_\beta\Omega^2}-8 & \gamma^m-\frac{32k_\beta}{\gamma^m I_\beta\Omega^2}\\ \frac{32k_\beta}{\gamma^m I_\beta\Omega^2}-\gamma^m & -\frac{4k_\beta}{I_\beta\Omega^2}-8\end{bmatrix}\begin{bmatrix}a\\ b\end{bmatrix}-\begin{bmatrix}q\\ p\end{bmatrix}+\frac{\gamma^m\Omega}{(\gamma^m)^2+64}\begin{bmatrix}8 & -\gamma^m\\ \gamma^m & 8\end{bmatrix}\begin{bmatrix}A_1^m+K_s a_s\\ B_1^m+K_s b_s\end{bmatrix},\\
\begin{bmatrix}\dot{a}_s\\ \dot{b}_s\end{bmatrix} &= \frac{\gamma^s\Omega}{(\gamma^s)^2+64}\begin{bmatrix}-8 & \gamma^s\\ -\gamma^s & -8\end{bmatrix}\begin{bmatrix}a_s\\ b_s\end{bmatrix}-\begin{bmatrix}q\\ p\end{bmatrix}+\frac{\gamma^s\Omega}{(\gamma^s)^2+64}\begin{bmatrix}8 & -\gamma^s\\ \gamma^s & 8\end{bmatrix}\begin{bmatrix}A_1^s\\ B_1^s\end{bmatrix},
\end{aligned}\tag{3}$$

where (a,b) and (a_s,b_s) are the flapping angles of the main blades and stabilizer in longitudinal and lateral directions, respectively; k_β is the spring constant of the rotor hub; γ^m is the lock number of the main blades; γ^s is the lock number of the stabilizer; I_β is the moment of inertia of the main blades; Ω is the rotation speed of the main rotor; and K_s is the mixer coefficient. (A_1^m,B_1^m) and (A_1^s,B_1^s) are the cyclic pitch angles of the main blade and stabilizer in longitudinal and lateral directions, respectively, which can be determined by the pitch angles of swash plate (A_1,B_1) easily through the following relations:

$$\begin{aligned}
A_1^m &= K_{\rm bel}A_1, \quad A_1^s = K_{\rm sb}A_1,\\
B_1^m &= K_{\rm bel}B_1, \quad B_1^s = K_{\rm sb}B_1,
\end{aligned}$$

where $K_{\rm bel}$ and $K_{\rm sb}$ are the mechanical gains from the swash plate to the main blade and stabilizer. The pitch angles of swash plate (A_1,B_1) satisfy

$$A_1 = K_{\rm lon}K_a\delta_{\rm lon}, \quad B_1 = K_{\rm lat}K_a\delta_{\rm lat},$$

where $K_{\rm lon}$ and $K_{\rm lat}$ are the linkage gains from the elevator and aileron actuators to the swash plate, respectively; K_a is the gain of the actuators (from the control signal to the deviation). The dynamics of the actuator is ignored and modeled as a constant gain K_a.

The main source of the control force is the main rotor. The thrust of the main rotor can be expressed by a momentum theory based iterative scheme [29]:

$$\begin{cases}
T = (w_b - v_i)\frac{\rho\Omega R^2 C_{l\alpha} b_m c_m}{4},\\
v_i^2 = \sqrt{\left(\frac{\bar{v}^2}{2}\right)^2+\left(\frac{T}{2\rho\pi R^2}\right)^2}-\frac{\bar{v}^2}{2},\\
\bar{v}^2 = u^2+v^2+w(w-2v_i),
\end{cases}\tag{4}$$

where

$$w_b = w+\frac{2}{3}\Omega R\theta_{\rm col}, \quad \theta_{\rm col} = K_{\rm col}K_a\delta_{\rm col}.$$

b_m is the number of the main blades; c_m is the chord length of the main blade; ρ is the air density; R is the radius of the main rotor; w_b is the resultant velocity at the main rotor in vertical direction; and $\theta_{\rm col}$ is the collective pitch angle. $\theta_{\rm col}$ is controlled by the collective actuator. $K_{\rm col}$ is the linkage gain from the collective actuator to the main blade. $\delta_{\rm col}$ is the control signal of the collective actuator.

The force components generated by the main rotor can be calculated as follows:

$$\begin{cases}
X_{\rm mr} = -T\sin a,\\
Y_{\rm mr} = T\sin b,\\
Z_{\rm mr} = -T\cos a\cos b.
\end{cases}\tag{5}$$

It is known that the dominating force is the thrust component of the main rotor along the z axis of the body frame, and the components in other directions are small and can be disregarded. Then

$$F_b = \begin{bmatrix}0 & 0 & -T\end{bmatrix}^{\rm T}.\tag{6}$$

Table 1 Model parameters of the small-scale helicopter [28]

Parameter	Value	Parameter	Value
m	7.495 kg	I_β	0.0913 kg $\cdot$ m^2
I_{xx}	0.1895 kg $\cdot$ m^2	γ^m	1.3112
I_{yy}	0.4515 kg $\cdot$ m^2	γ^s	0.3282
I_{zz}	0.3408 kg $\cdot$ m^2	k_β	167.6592
$C_{l\alpha}$	4.0734	R	0.785 m
c_m	0.06 m	K_a	9.4248
$K_{\rm bel}$	0.4825	$K_{\rm sb}$	1.1959
$K_{\rm lon}$	0.4667	$K_{\rm lat}$	0.4434
$H_{\rm mr}$	0.275 m	–	–

The moments generated by the main rotor along x and y body axes are given by

$$\begin{cases} L_{\rm mr} = (k_\beta + TH_{\rm mr}) \sin b, \\ M_{\rm mr} = (k_\beta + TH_{\rm mr}) \sin a. \end{cases} \tag{7}$$

Generally, it can be assumed that $\sin a \approx a$ and $\sin b \approx b$ because the flapping angles are often very small. In this paper, it is assumed that $L_{\rm mr}$ and $M_{\rm mr}$ are the primary control moments in roll and pitch channels, and other small components are neglected.

For a small-scale helicopter, yaw direction control in manual flight is very challenging due to the high control sensitivity and the coupling effect between the main rotor and tail rotor. To overcome this problem, an Angular Vector Control System (AVCS) is installed to facilitate manual control in our platform and it is reserved for flight control design. Then, the yaw control moment can be disregarded and the torques exerted on the small-scale helicopter can be written as follows:

$$M_b = \begin{bmatrix} (k_\beta + TH_{\rm mr})b \\ (k_\beta + TH_{\rm mr})a \\ 0 \end{bmatrix}. \tag{8}$$

The model parameters are determined by system identification [28] and presented in Table 1. The objective of this paper is to design the control inputs $u = [\delta_{\rm lon}, \delta_{\rm lat}]$ to force the roll and pitch to converge to the reference signals. Actually, $\delta_{\rm lon}$ and $\delta_{\rm lat}$ represent the duty of PWM control signals, which can be directly applied to the motors. We assume that the existing heave controller and AVCS can yield ideal performance and the corresponding effect can be disregarded.

3 Controller design

In this section, a nonlinear robust roll and pitch controller is proposed. Firstly, the flapping dynamics expressed in (3) is simplified as a lumped model. Then, the inner loop angular rate controller and outer loop attitude controller are designed based on the lumped flapping model.

3.1 Lumped flapping dynamics

As mentioned in Introduction, the flapping motion affects system dynamics heavily. Therefore, considering flapping dynamics during controller design is very significative for improving control performance. A practical method is disregarding flapping dynamics and treating it as a quasi-steady state equation, then the flapping motion can be expressed by a algebraic relationship, named quasi-steady flapping model [16, 24, 27]. However, this method can not reflect the flapping dynamical characteristics, and will discount control performance; on the other hand, the full-order flapping model expressed by (3) is too

complicated, designing a controller based on which is impractical. In this paper, we adopt a lumped model to depict the flapping dynamics, which can simplify the controller design problem.

Based on (3), we define the first-order main blades flapping time constant τ_m and stabilizer bar flapping time constant τ_s as follows:

$$\tau_m = \frac{I_\beta \Omega[(\gamma^m)^2 + 64]}{\gamma^m(4k_\beta + 8I_\beta\Omega^2)}, \quad \tau_s = \frac{(\gamma^s)^2 + 64}{8\gamma^s\Omega}.$$

Generally, τ_s (about 0.1412 s) is several times larger than τ_m (about 0.0352 s), and the dominating dynamics is the stabilizer bar flapping dynamics in (3). The flapping dynamics in (3) can be simplified as lumped flapping dynamics [26]. Consider the main blades flapping dynamics as steady ($\dot{a} = 0$ and $\dot{b} = 0$), the first equation of (3) can be transformed as

$$\beta_m = B_{m\omega}\omega_1 + B_{ms}\beta_s + B_{mu}u_1, \tag{9}$$

where $\beta_m = [a, b]^{\mathrm{T}}$ is the main rotor flapping angle vector, $\beta_s = [a_s, b_s]^{\mathrm{T}}$ is the stabilizer bar flapping angle vector, and $u_1 = [A_1, B_1]^{\mathrm{T}}$ is the cyclic pitch angles of the swash plate. $B_{m\omega}$, B_{ms} and B_{mu} can be directly calculated:

$$B_{m\omega} = \left(\frac{\gamma^m\Omega}{(\gamma^m)^2+64}\Gamma\right)^{-1}\begin{bmatrix}0 & 1\\ 1 & 0\end{bmatrix}, \quad B_{ms} = -\Gamma^{-1}K_s\begin{bmatrix}8 & -\gamma^m\\ \gamma^m & 8\end{bmatrix},$$
$$B_{mu} = -\Gamma^{-1}K_{\mathrm{bel}}\begin{bmatrix}8 & -\gamma^m\\ \gamma^m & 8\end{bmatrix}, \quad \Gamma = \begin{bmatrix}-\frac{4k_\beta}{I_\beta\Omega^2} - 8 & \gamma^m - \frac{32k_\beta}{\gamma^m I_\beta\Omega^2}\\ \frac{32k_\beta}{\gamma^m I_\beta\Omega^2} - \gamma^m & -\frac{4k_\beta}{I_\beta\Omega^2} - 8\end{bmatrix}.$$

The stabilizer bar dynamics also can be expressed as

$$\dot{\beta}_s = A_s\beta_s + B_{s\omega}\omega_1 + B_{su}u_1, \tag{10}$$

where A_s, $B_{s\omega}$ and B_{su} are corresponding to the matrixes in the second equation of (3):

$$A_s = \frac{\gamma^s\Omega}{(\gamma^s)^2+64}\begin{bmatrix}-8 & \gamma^s\\ -\gamma^s & -8\end{bmatrix}, \quad B_{s\omega} = \begin{bmatrix}0 & -1\\ -1 & 0\end{bmatrix}, \quad B_{su} = \frac{\gamma^s\Omega}{(\gamma^s)^2+64}\begin{bmatrix}8 & -\gamma^s\\ \gamma^s & 8\end{bmatrix}.$$

Expressing (10) in transfer function form and substituting it into (9) yield

$$\beta_m = B_{m\omega}\omega_1 + B_{ms}(sI - A_s)^{-1}(B_{s\omega}\omega_1 + B_{su}u_1) + B_{mu}u_1. \tag{11}$$

With the left multiplication of $(sI - A_s)B_{ms}^{-1}$ on both sides of (11), we obtain

$$(sI - A_s)B_{ms}^{-1}\beta_m = (sI - A_s)B_{ms}^{-1}(B_{m\omega}\omega_1 + B_{mu}u_1) + B_{s\omega}\omega_1 + B_{su}u_1. \tag{12}$$

Applying the inverse Laplace transform to (12) and disregarding the small terms (the derivatives of ω_1 and u_1), the lumped flapping dynamics finally can be expressed as

$$\dot{\beta}_m = A\beta_m + B_\omega\omega_1 + B_u u_1, \tag{13}$$

where

$$A = B_{ms}A_sB_{ms}^{-1},$$
$$B_\omega = B_{ms}(B_{s\omega} - A_sB_{ms}^{-1}B_{m\omega}),$$
$$B_u = B_{ms}(B_{su} - A_sB_{ms}^{-1}B_{mu}).$$

Assume that the helicopter works at hover and the main rotor thrust $T = T_h = mg$, taking the roll channel as an example and disregarding the nonlinear cross product of the angular rates in (1), the roll dynamics then can be described as

$$\dot{p} = L_b b, \tag{14}$$

where $L_b = (k_\beta + T_h H_{\mathrm{mr}})/I_{xx}$. Figure 3 shows the roll response comparison among the full-order, lumped and quasi-steady models, which clearly indicates that (13) can accurately capture the dynamic characteristics of the full-order flapping dynamics, and the quasi-steady model is unsuitable at higher bandwidths. Therefore, it is necessary to consider the flapping dynamics for control design.

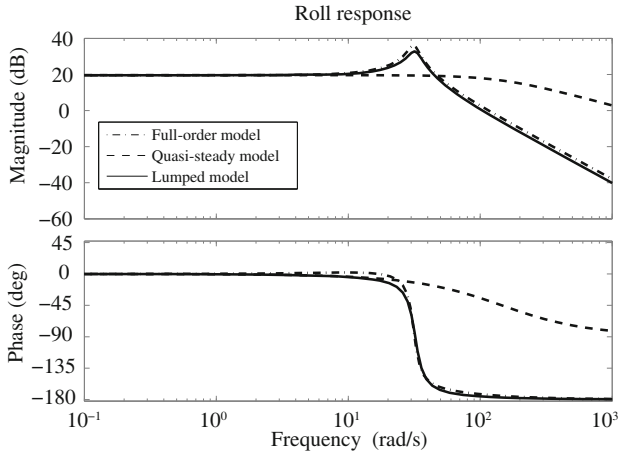

Figure 3 Roll response comparison among the full-order, lumped and quasi-steady models.

3.2 Angular rates control

Based on the analysis in Subsection 3.1, we propose a novel angular rates controller in this section, in which the flapping dynamics is explicitly considered. A state transformation is introduced to avoid observing the flapping angles directly, and second-order sliding mode technique is adopted to compensate for the uncertainties incorporating with extended state observer (ESO), which is a kernel technique of active disturbance rejection control [30]. The basic idea is treating the disturbances as extended states and designing an observer to estimate them.

3.2.1 *Extended state observer design*

Considering the model uncertainties $\Delta_2(\omega_1, r)$, the lumped flapping dynamics in (13) is modified as

$$\dot{\beta}_m = A\beta_m + B_\omega \omega_1 + B_u u_1 + \Delta_2(\omega_1, r). \tag{15}$$

Combining (1) and (7), we can write the roll and pitch dynamics as

$$\dot{\omega}_1 = k_I(k_\beta + TH_{\rm mr})\beta_m + f_1(\omega_1, r) + f_{\Delta 1}(\omega_1, r), \tag{16}$$

where $f_1(\omega_1, r)$ denotes the nonlinear cross product of angular rates, $f_{\Delta 1}$ denotes the parametric uncertainties, and k_I is a constant matrix related to the moments of inertia:

$$k_I = \begin{bmatrix} 0 & \frac{1}{I_{xx}} \\ \frac{1}{I_{yy}} & 0 \end{bmatrix}.$$

In (16), the main rotor thrust T is required, which cannot be accurately obtained in real time. To simplify the design, we start control design from hover mode. Therefore, the roll and pitch rotation dynamics of the small-scale helicopter can be written as

$$\begin{cases} \dot{\omega}_1 = k_I(k_\beta + T_h H_{\rm mr})\beta_m + \Delta_1(\omega_1, r), \\ \dot{\beta}_m = A\beta_m + B_\omega \omega_1 + B_u u_1 + \Delta_2(\omega_1, r), \end{cases} \tag{17}$$

where $T_h = mg$ is the main rotor thrust at hover, $\Delta_1(\omega_1, r)$ denotes the lumped uncertainties defined as follows:

$$\Delta_1(\omega_1, r) = f_1(\omega_1, r) + f_{\Delta 1}(\omega_1, r) + k_I(T - T_h)H_{\rm mr}\beta_m.$$

Apparently, the relative order of (17) is $\{2, 2\}$. Two factors make the control problem difficult: the mis-matched uncertainty $\Delta_1(\omega_1, r)$ in the first equation of (17) and the immeasurability of the flapping angles. To overcome these difficulties, a state transformation is introduced, so that

$$x = T(z), \;\; x = \begin{bmatrix} \omega_1 & \dot{\omega}_1 \end{bmatrix}^{\rm T}, \;\; z = \begin{bmatrix} \omega_1 & \beta_m \end{bmatrix}^{\rm T}.$$

It is reasonable to assume that $\Delta_1(\omega_1, r)$ is first-order differentiable, because all the factors of $\Delta_1(\omega_1, r)$ are generally smooth. Then, the dynamics in (17) can be rewritten as follows:

$$\begin{cases} \dot{x}_1 = x_2, \\ \dot{x}_2 = k_\omega B_\omega x_1 + k_\omega B_u u_1 + \Delta_t, \end{cases} \tag{18}$$

where $k_\omega = k_I(k_\beta + T_h H_{\rm mr})$, and $\Delta_t = k_\omega A\beta_m + k_\omega \Delta_2(\omega_1, r) + \dot{\Delta}_1(\omega_1, r)$ is the total disturbances need to be compensated.

For the system in (18), we can design an extended state observer to provide the estimates of Δ_t and x_2. Define the extended state $x_3 = \Delta_t$, the system is extended as

$$\begin{cases} \dot{x}_1 = x_2, \\ \dot{x}_2 = k_\omega B_\omega x_1 + k_\omega B_u u_1 + x_3, \\ \dot{x}_3 = h(t). \end{cases} \tag{19}$$

Then the corresponding extended state observer used in this work is designed as follows:

$$\begin{cases} \dot{\hat{x}}_1 = \hat{x}_2 - L_1(\hat{x}_1 - x_1), \\ \dot{\hat{x}}_2 = k_\omega B_\omega \hat{x}_1 + k_\omega B_u u_1 + \hat{x}_3 - L_2(\hat{x}_1 - x_1), \\ \dot{\hat{x}}_3 = -L_3(\hat{x}_1 - x_1), \end{cases} \tag{20}$$

where $L_1,\ L_2,\ L_3$ are the observer gain matrixes, and $\hat{}$ denotes the estimate of the variable, $\hat{x}_3 = [\hat{\chi}_1, \hat{\chi}_2]^{\rm T}$ is the estimate of the total disturbances. It has been proven in [31] that the estimation errors of (20) are bounded with appropriate selection of $L_1,\ L_2,\ L_3$. Substantially, Eq. (20) is a high gain observer, and the selection of observer gain is similar.

3.2.2 *Second-order sliding mode control design*

The control law is defined as

$$u_1 = u_n + u_c, \tag{21}$$

where u_n is the nominal control law, and u_c is the compensation control law. u_n is designed for the nominal condition that the extended state observer can accurately estimate the system states and total disturbances: $\hat{x}_2 = x_2,\ \hat{x}_3 = x_3$. Actually, the nominal control law based on extended state observer can compensate a large part of uncertainties. However, the extended state observer cannot eliminate estimation errors. u_c is designed to compensate for the residual uncertainties.

The nominal control law is selected as

$$u_n = -(k_\omega B_u)^{-1}(k_\omega B_\omega x_1 - v_n) - (k_\omega B_u)^{-1}\hat{x}_3, \tag{22}$$

where v_n is the nominal pseudo control. Substituting (21) into (19), the roll and pitch rotation dynamics can be simplified as

$$\begin{cases} \dot{x}_1 = x_2, \\ \dot{x}_2 = v_n + \Delta_r + k_\omega B_u u_c, \end{cases} \tag{23}$$

where $\Delta_r = -\tilde{x}_3 + \Delta_o$ denotes the residual uncertainties, $\tilde{x}_3 = \hat{x}_3 - x_3$, and Δ_o represents other disturbances.

In hope of enhancing robustness, we adopt the second-order sliding mode method to cope with the residual uncertainties in (23). Defining the sliding variable as $s = \omega_{1r} - \omega_1$, the second-order sliding mode control problem is designing a suitable control function to stabilize the system to the following second-order sliding set in finite time:

$$\Sigma^2 = \{\omega_1 | s = \dot{s} = 0\}.$$

Define the error vector as $[e_1, e_2]^{\rm T} = [s, \dot{s}]^{\rm T}$. For the nominal control problem, we have the following theorem:

Theorem 1. Assume that the ESO (20) can accurately estimate the states and disturbances, for the nominal condition ($\Delta_r = 0$ and $u_c = 0$ in (23)), design the pseudo nominal control as

$$v_n = \ddot{\omega}_{1r} + k_p |e_1|^{\alpha_1} \operatorname{sign}(e_1) + k_d |e_2|^{\alpha_2} \operatorname{sign}(e_2), \tag{24}$$

where $k_p, k_d > 0$, $0 < \alpha_2 < 1$ and $\alpha_1 = \alpha_2/(2-\alpha_2)$. Then, Eq. (23) is globally finite-time stable.

Proof. Substituting (24) into (23), the error dynamics can be concluded as

$$\begin{cases} \dot{e}_1 = e_2, \\ \dot{e}_2 = -k_p |e_1|^{\alpha_1} \operatorname{sign}(e_1) - k_d |e_2|^{\alpha_2} \operatorname{sign}(e_2). \end{cases} \tag{25}$$

Define the Lyapunov function candidate as

$$V_1 = \frac{k_p |e_1|^{\alpha_1+1}}{\alpha_1 + 1} + \frac{|e_2|^2}{2}. \tag{26}$$

Differentiating (26) yields

$$\dot{V}_1 = k_p |e_1|^{\alpha_1} \operatorname{sign}(e_1)\dot{e}_1 + |e_2| \operatorname{sign}(e_2)\dot{e}_2. \tag{27}$$

Substituting (25), the above equation can be simplified as

$$\dot{V}_1 = -k_d |e_2|^{\alpha_2+1}. \tag{28}$$

Obviously, $\dot{V}_1 \leqslant 0$. According to Barbalat Lemma, it is easy to conclude that $\dot{V}_1 \to 0$ and $e_1, e_2 \to 0$. Additionally, let $r_1 = 1$, $r_2 = 1/(2-\alpha_2)$ and $0 < \alpha_2 < 1$, the homogeneous of degree of (25) with respect to the dilation, $(e_1, e_2) \mapsto (k^{r1}e_1, k^{r2}e_2)$, is $(\alpha_2 - 1)/(2-\alpha_2) < 0$, that means (25) is globally finite-time stable.

The above theorem proposes the control law for the nominal condition, which substantially is a reference signal need to be tracked by the actual system. However, the ESO is impossible to compensate for the uncertainties completely and there exists residual uncertainties. To compensate for the effect of residual uncertainties, we define a new sliding variable:

$$\sigma = x_2 - \int_0^{\mathrm{T}} v_n \mathrm{d}\tau. \tag{29}$$

And the compensation pseudo control is designed as

$$v_c = -\beta \operatorname{sign}(\sigma), \tag{30}$$

where $\beta = \operatorname{diag}\{\beta_1, \beta_2\}$ and $\beta_i > \|\Delta_{ri}\| + \varepsilon_i, \varepsilon_i > 0$ for $i = 1, 2$. Then, the corresponding compensation control law is

$$u_c = -(k_\omega B_u)^{-1} \beta \operatorname{sign}(\sigma). \tag{31}$$

Theorem 2. For the roll and pitch dynamics (19), select the control law as (21), where u_n and u_c are designed as (22) and (31), respectively. Then, the system (23) can reach the second-order sliding set Σ^2 in finite time under the general condition.

Proof. Select the Lyapunov function candidate as

$$V_2 = \frac{1}{2}\sigma^{\mathrm{T}}\sigma. \tag{32}$$

Differentiating V_2 along (23), we can get

$$\begin{aligned} \dot{V}_2 &= \sigma^{\mathrm{T}}\dot{\sigma} = \sigma^{\mathrm{T}}(\dot{x}_2 - v_n) = \sigma^{\mathrm{T}}(-\beta \operatorname{sign}(\sigma) + \Delta_r) \\ &\leqslant -\varepsilon_m \|\sigma\| = -\varepsilon_m \sqrt{2} V_2^{\frac{1}{2}}, \end{aligned} \tag{33}$$

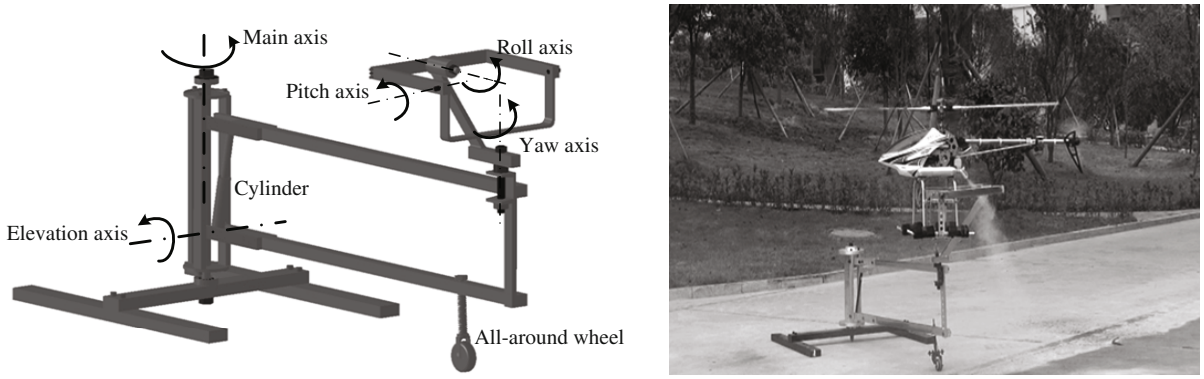

Figure 4 Flight experiment stand.

where $\varepsilon_m = \min\{\varepsilon_1, \varepsilon_2\}$. According to comparison lemma [32], we can conclude that σ can arrive at 0 in finite time. Meanwhile, v_n is designed according to Theorem 1. Therefore, the second-order sliding mode with respect to s can be established in finite time.

Actually, Theorem 1 is used to derive the nominal pseudo control v_n and the goal of the compensation control law (31) is to force $\dot{x}_2$ to arrive at v_n. The flapping angle feedback is realized by introducing $\dot{\omega}_1$ feedback, since $(\omega_1, \dot{\omega}_1)$ is equivalent to (ω_1, β_m). Additionally, x_2 is replaced by its estimation $\hat{x}_2$ in (43), the corresponding estimation error has been included in Δ_o. For practical implementation, saturation function is used to replace the sign to decrease the chattering effect.

3.3 Attitude control

Actually, the attitude kinematics is much slower than the rotation dynamics, we can then design attitude controller independently. Based on (1) and (2), the roll and pitch kinematics can be rewritten as

$$\dot{\Theta} = A_\Theta \omega_1 + B_\Theta r, \tag{34}$$

where

$$A_\Theta = \begin{bmatrix} 1 & \sin\phi\tan\theta \\ 0 & \cos\phi \end{bmatrix}, \quad B_\Theta = \begin{bmatrix} \cos\phi\tan\theta \\ -\sin\phi \end{bmatrix}.$$

Here, we choose ω_1 as the virtual control input of (34), and define the pseudo control v_Θ as

$$v_\Theta = \dot{\Theta}_r + k_\Theta(\Theta_r - \Theta), \tag{35}$$

where Θ_r is the reference signal of Θ, k_Θ is a positive matrix. Then, the desired angular rate ω_{1r} can be selected as

$$\omega_{1r} = A_\Theta^{-1}(v_\Theta - B_\Theta r). \tag{36}$$

4 Experiments and results

Two flight experiments have been carried out to investigate the control performance of the proposed scheme on the real helicopter. To facilitate experiment implementation and to guarantee the safety of the helicopter, we construct a five DOFs flight experiment stand in this paper [33], as shown in Figure 4. The stand is a mechanical construction able to hold a helicopter, allowing basic movements while protecting it from damaging and crashing. The roll, pitch and yaw axes provide the whole DOFs of rotation, and the main and elevation axes provide two DOFs of translation. The helicopter is fixed on the stand when flying and the influences of the stand are treated as disturbances which can be estimated by the ESO in this paper.

For safety, all the external commands in the experiments are generated by the pilot through RC controller. The positions of controller sticks are corresponding to the desired attitude angles. Each

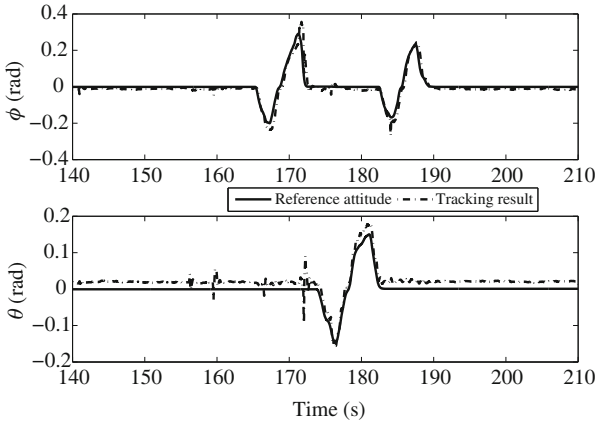

Figure 5 Tracking results without compensation.

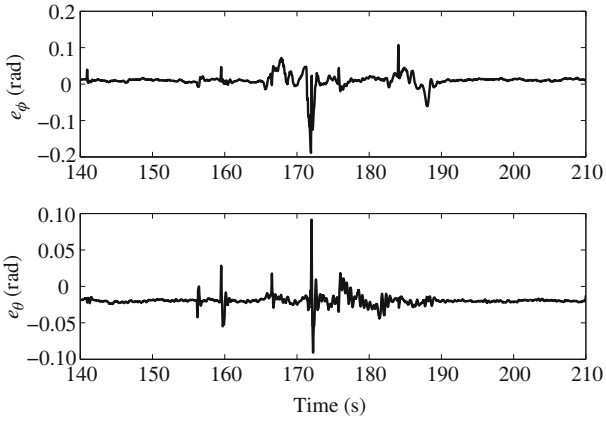

Figure 6 Tracking errors without compensation.

experiment includes two parts: for the first part, the helicopter is kept in hover mode, which is mainly used to validate the stabilizing performance; and the second part is designed to check the tracking performance of the proposed controller, in which the helicopter is controlled maneuvering in the roll and pitch channels.

The nominal pseudo control in (24) adopts the following exponential function of errors

$$s(e_i) = |e_i|^{\alpha_i} \operatorname{sign}(e_i), \quad i = 1, 2. \tag{37}$$

However, the derivative of $s(e_i)$ at 0 is infinite when $0 < \alpha_i < 1$, which will introduce control chattering. For practical implementation, we use the following function to replace it, where δ_i is a positive constant.

$$s(e_i) = \begin{cases} |e_i|^{\alpha_i} \operatorname{sign}(e_i), & |e_i| > \delta_i, \\ e_i/\delta_i^{1-\alpha_i}, & |e_i| \leqslant \delta_i. \end{cases} \tag{38}$$

The controller parameters are set as

$$\alpha_2 = \frac{1}{3}, \quad k_\Theta = \begin{bmatrix} 5 & 0 \\ 0 & 5 \end{bmatrix}, \quad k_d = \begin{bmatrix} 80 & 0 \\ 0 & 40 \end{bmatrix}, \quad k_p = \begin{bmatrix} 200 & 0 \\ 0 & 200 \end{bmatrix}, \quad \delta_1 = \delta_2 = 0.05.$$

The first experiment is designed to validate the situation without disturbance compensation, that means u_c is removed from (21) and the disturbance estimate $\hat{x}_3$ is removed from (22). The experiment results are given in Figures 5–8. There are two parts: the first part is from 140 s to 165 s, the reference signals are kept at 0 rad; the second part is from 165 s to 210 s, the helicopter is controlled to track the reference roll and pitch angles. Figures 5 and 6 indicate that there exists steady-state errors, especially in the pitch channel (about 0.02 rad). Figures 7 and 8 are the angular rate results and corresponding control inputs, respectively. Although the controller without u_c and $\hat{x}_3$ in this experiment can track the reference signals modestly, but its control performance still need to be improved. It is clear that the control performance need to be improved although the control law determined only by the nominal model can modestly track the reference signals.

The second experiment is used to validate the whole controller, the disturbance compensation is included. To verify the merits of the proposed method, the experimental results based on the controller proposed in [28] are also presented for comparison, which does not consider the main rotor flapping dynamics.The results are given in Figures 9–15. Figures 9 and 10 are the experimental results of the controller in [28]. The whole experiment includes two phases: the first phase is from 470 s to 490 s, in which the reference signals are kept at 0 rad; and the second phase is from 490 s to 530 s, in which the helicopter is controlled to track the reference roll and pitch angles. Figures 11–15 are the experimental results of the proposed controller in this paper. From 210 s to 240 s, the reference signals are kept at 0 rad; From 240 s to 280 s, the helicopter is controlled to track the reference roll and pitch angles.

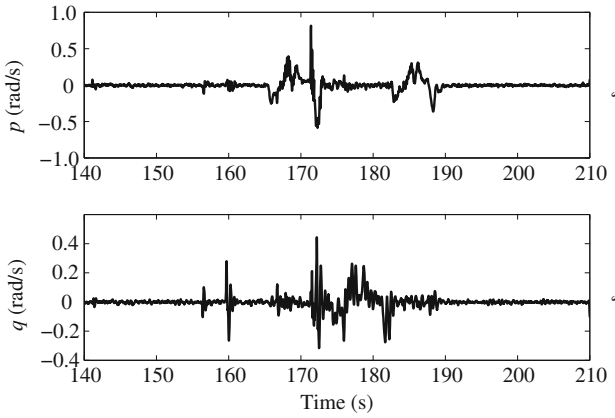

Figure 7 Tracking results without compensation.

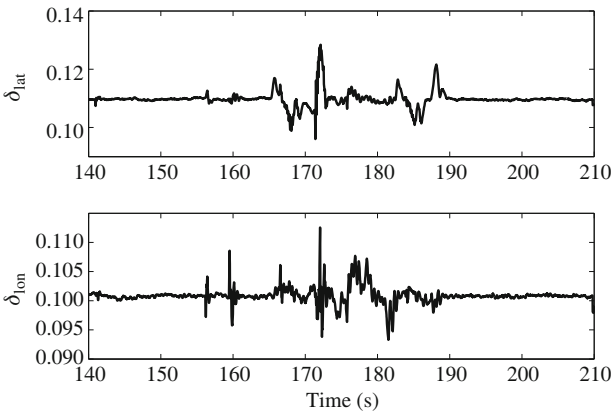

Figure 8 Control inputs without compensation.

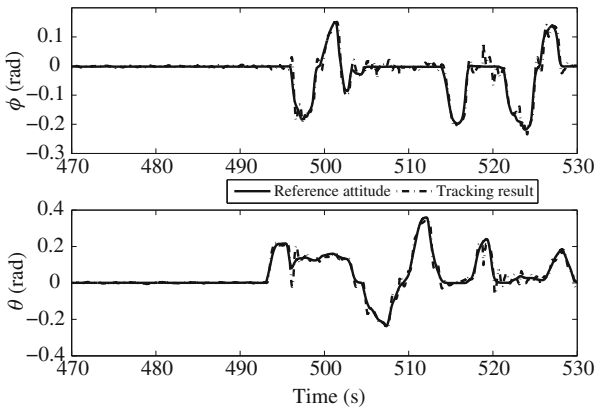

Figure 9 Tracking results of the controller in [28].

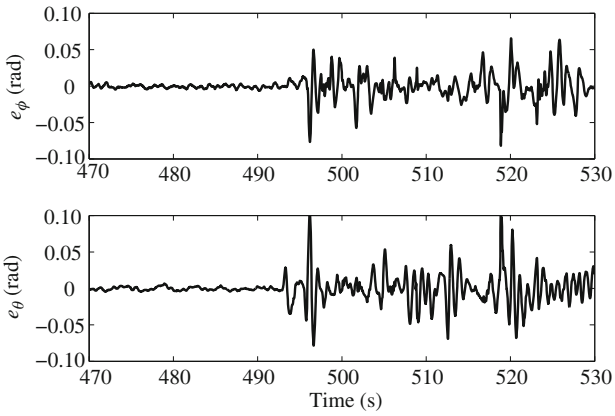

Figure 10 Tracking errors of the controller in [28].

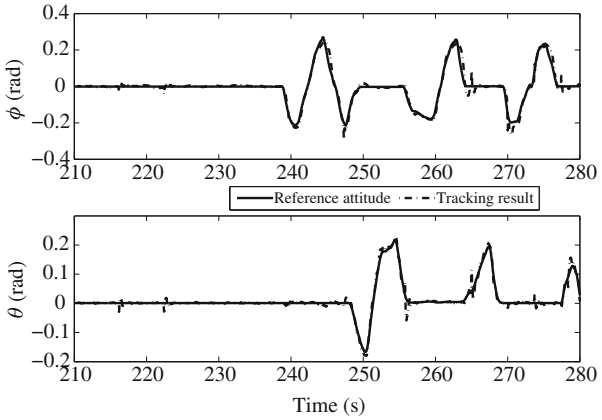

Figure 11 Tracking results with compensation.

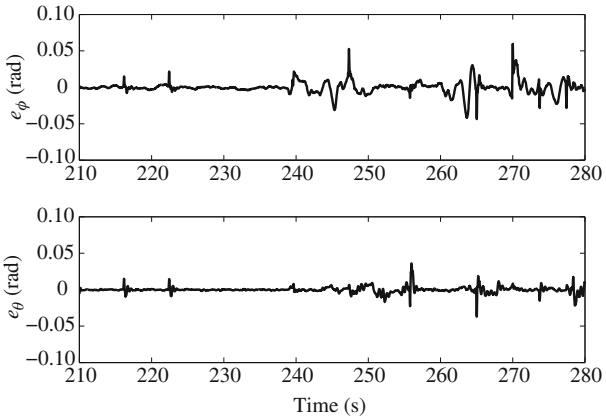

Figure 12 Tracking errors with compensation.

Figures 11 and 12 indicate that the disturbance compensation can eliminate the steady-state errors and improve the tracking performance. Compared with the results in Figures 9 and 10, we can conclude that the proposed controller in this paper yields smaller errors and better tracking performance. Figures 13 and 14 are the angular rate results and corresponding control inputs, respectively. Figure 15 is the result of the total disturbance estimation, which is the output of the ESO. The experiment results show that the proposed controller is effective.

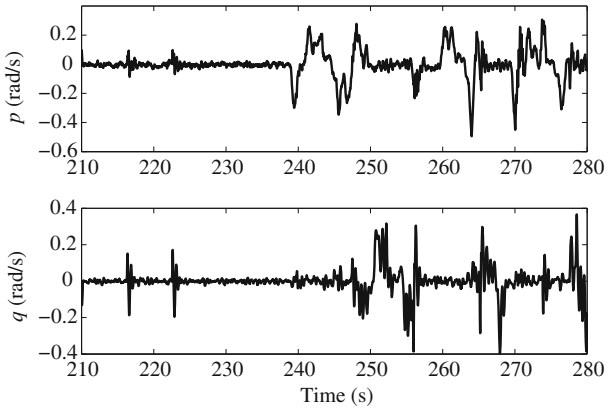

Figure 13 Angular rates with compensation.

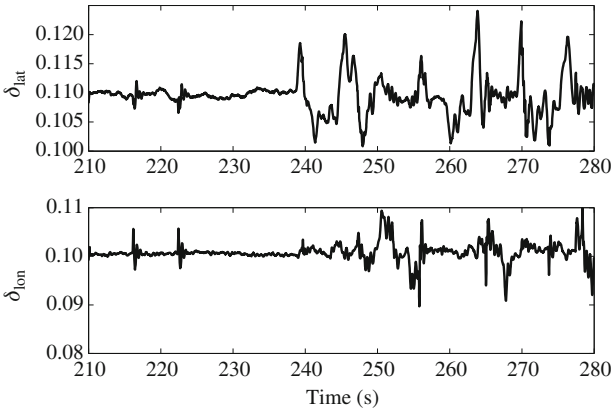

Figure 14 Control inputs with compensation.

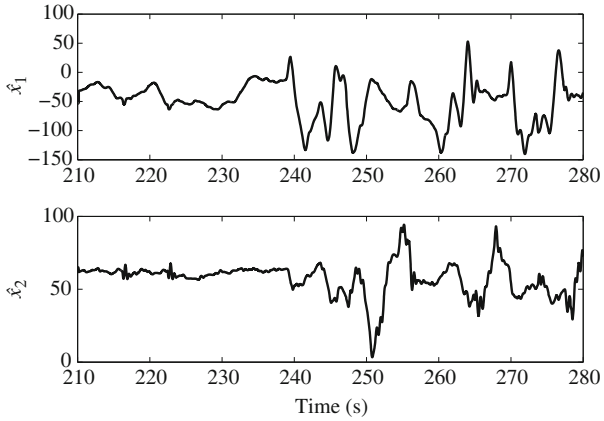

Figure 15 Disturbance estimation results with compensation.

5 Conclusion

This paper proposes a nonlinear robust roll and pitch controller of a small-scale helicopter, which adopts the second-order sliding mode method incorporating with extended state observer. To improve the control performance, the flapping dynamics of the main rotor is explored explicitly by introducing an equivalent state transformation. Considering the second-order characteristics of the angular dynamics, the second-order sliding mode method is adopted for angular control design. Extended state observer is used to estimate the immeasurable states and disturbance. The control performance and robustness of the proposed controller have been demonstrated by the experimental results.

Acknowledgements This work was supported by Basic and Advanced Research Project of Chongqing (Grant No. cstc2016jcyjA0563).

Conflict of interest The authors declare that they have no conflict of interest.

References

1 Sanada Y, Torii T. Aerial radiation monitoring around the fukushima dai-ichi nuclear power plant using an unmanned helicopter. J Environ Radioact, 2014, 139: 294–299
2 Siebert S, Teizer J. Mobile 3D mapping for surveying earthwork projects using an unmanned aerial vehicle (UAV) system. Autom Constr, 2014, 41: 1–14
3 Maza I, Kondak K, Bernard M, et al. Multi-UAV cooperation and control for load transportation and deployment. J Intell Robot Syst, 2010, 57: 417–449
4 Maza I, Caballero F, Capitán J, et al. Experimental results in multi-UAV coordination for disaster management and civil security applications. Int J Syst Sci, 2011, 61: 563–585

5 Casbeer D W, Kingston D B, Beard A W, et al. Cooperative forest fire surveillance using a team of small unmanned air vehicles. Int J Syst Sci, 2006, 37: 351–360
6 Bernard M, Kondak K, Hommel G, et al. Attitude control optimization for a small-scale unmanned helicopter. In: Proceedings of AIAA Guidance, Navigation, and Control Conference and Exhibit, Denver, 2000. AIAA-2000-4059
7 Brown A, Garcia R. Concepts and validation of a small-scale rotorcraft proportional integral derivative (PID) controller in a unique simulation environment. Int J Syst Sci, 2009, 54: 511–532
8 Gavrilets V. Autonomous aerobatic maneuvering of miniature helicopters. Dissertation for Doctoral Degree. Massachusetts Institute of Technology, 2003
9 Gavrilets V, Mettler B, Feron E. Human-inspired control logic for automated maneuvering of miniature helicopter. J Guid Control Dyn, 2004, 27: 752–759
10 Cai G W, Chen B M, Dong X X, et al. Design and implementation of a robust and nonlinear flight control system for an unmanned helicopter. Mechatronics, 2011, 21: 803–820
11 La Civita M. Integrated modeling and robust control for full-envelope flight of robotic helicopter. Dissertation for Doctoral Degree. Carnegie Mellon University, 2002
12 Pota H R, Ahmed B, Garratt M. Velocity control of a UAV using backstepping control. In: Proceedings of the 45th IEEE Conference on Decision and Control, San Diego, 2006. 5894–5899
13 Ahmed B, Pota H R, Garratt M. Rotary wing UAV position control using backstepping. In: Proceedings of the 46th IEEE Conference on Decision and Control, New Orleans, 2007. 1957–1962
14 Ahmed B, Pota H R. Flight control of a rotary wing UAV using adaptive backstepping. In: Proceedings of IEEE International Conference on Control and Automation, Christchurch, 2009. 1780–1785
15 Lee C-T, Tsai C-C. Improvement in trajectory tracking control of a small scale helicopter via backstepping. In: Proceedings of International Conference on Mechatronics, Kumamoto, 2007. 1–6
16 Lee C-T, Tsai C-C. Nonlinear adaptive aggressive control using recurrent neural networks for a small scale helicopter. Mechatronics, 2010, 20: 474–484
17 Li P, Zheng Z-Q. Robust adaptive second-order sliding-mode control with fast transient performance. IET Control Theory A, 2012, 6: 305–312
18 Li P. Research and application of traditional and higher-order sliding mode control (in Chinese). Dissertation for Doctoral Degree. National University of Defense Technology, 2011
19 Xia Y Q, Zhu Z, Fu M Y, et al. Attitude tracking of rigid spacecraft with bounded disturbances. IEEE Trans Ind Electron, 2011, 58: 647–659
20 Xu Y J. Multi-timescale nonlinear robust control for a miniature helicopter. IEEE Trans Aerosp Electron Syst, 2010, 46: 656–671
21 Lei X S, Sam Ge S Z, Fang J C. Adaptive neural network control of small unmanned aerial rotorcraft. Int J Syst Sci, 2014, 75: 331–341
22 Song B Q, Liu Y H, Fan C Z. Feedback linearization of the nonlinear model of a small-scale helicopter. J Control Theory Appl, 2010, 8: 301–308
23 Cai G W, Chen B M, Peng K M, et al. Modeling and control of the yaw channel of a UAV helicopter. IEEE Trans Ind Electron, 2008, 55: 3426–3434
24 Liu C J, Chen W H, Andrews J. Tracking control of small-scale helicopters using explicit nonlinear MPC augmented with disturbance observers. Control Eng Pract, 2012, 20: 258–268
25 Liu C J, Chen W H, Andrews J. Piecewise constant model predictive control for autonomous helicopters. Robot Auton Syst, 2011, 59: 571–579
26 Mettler B. Identification Modeling and Characteristics of Miniature Rotorcraft. New York: Springer US, 2003
27 Zhou H B. Small-scale unmanned helicopter modeling and controller design (in Chinese). Dissertation for Doctoral Degree. South China University of Technology, 2011
28 Tang S, Zheng Z Q, Qian S K, et al. Nonlinear system identification of a small-scale unmanned helicopter. Control Eng Pract, 2014, 25: 1–15
29 Cai G W, Chen B M, Lee T H, et al. Comprehensive nonlinear modeling of an unmanned-aerial-vehicle helicopter. In: Proceedings of AIAA Guidance, Navigation and Control Conference and Exhibit, Honolulu, 2008. AIAA-2008-7414
30 Han J Q. Active Disturbance Rejection Control Technique—The Technique for Estimating and Compensating the Uncertainties (in Chinese). Beijing: National Defense Industry Press, 2008
31 Chen Z Q, Sun M W, Yang R G. Research on the stability of linear active disturbance rejection control (in Chinese). Acta Automat Sin, 2013, 39: 574–580
32 Khalil H K. Nonlinear System. Englewood Cliffs: Prentice Hall Inc., 1996
33 Vitzilaios N I, Tsourveloudis N C. An experimental test bed for small unmanned helicopters. J Intell Robot Syst, 2009, 54: 769–794